Thermodynamic Analysis and Synthesis of Zirconium Nitride by Thermal Nitridation of Sol-Gel Zirconium Oxide

Beng Jit Tan,[†,‡] Youming Xiao,[†] Francis S. Galasso,[†] and Steven L. Suib*[,†,‡]

Department of Chemistry and Institute of Materials Science, U-60, University of Connecticut, Storrs, Connecticut 06269-3060

Received December 6, 1993. Revised Manuscript Received April 15, 1994®

Thermodynamic calculations were performed using the SOLGASMIX-PV computer program to predict the possibility of converting zirconia to zirconium nitride by thermal nitridation in the presence of methane and ammonia. Conversion diagrams were constructed for the ZrO_2–NH_3–CH_4 system over a range of reaction conditions such as temperature, total system pressure, and reagent concentrations. Formation of pure ZrN phase was predicted in the range 1800–2000 K and total system pressures of 0.1–1.0 atm. It is shown experimentally, in the present work, that zirconium nitride can indeed be synthesized by thermal nitridation of zirconia using ammonia and methane at a reaction temperature much lower than that predicted by thermodynamic considerations alone. In addition, no deposition of carbon was observed at the lower temperatures employed during synthesis. Low pressure together with the introduction of excess hydrogen favors the conversion of zirconia to zirconium nitride as well as decrease the reaction temperature for conversion to take place.

Introduction

In recent years, there has been increasing interest in non-oxide ceramics such as metal nitrides and carbides that possess high-temperature strength and corrosion resistance. Among these materials, zirconium nitride is especially important because of its unique physical properties. For example, zirconium nitride exhibits metallic behavior with low electrical resistance,[1] extreme hardness and wear resistance,[2] high melting point (ca. 3000 °C),[3] remarkable chemical and corrosion resistance,[4] and low-temperature superconductivity.[5] These properties displayed by zirconium nitride provide for its many potential applications. For example, it can be used as wear resistant, friction reducing coatings for machine tools[2,6] and gold-colored decorative coatings.[7] Also, its optical properties make it suitable for use as wavelength-selective transparent optical films[8] and solar control coatings for windows.[9] In microelectronic devices, zirconium nitride films are used as low-resistance contacts and diffusion barriers in interconnect metallization schemes.[10,11] Zirconium nitride films were reported to be successfully used as coatings for thermometers in cryogenic work.[12] Zirconium nitride has also been proposed for use in low-barrier Schottky diodes and as the gate electrode in MOS transistors.[13]

Zirconium nitride can be synthesized using a variety of techniques. For example, tribiological and cosmetic coatings have been prepared by chemical vapor deposition (CVD).[14] For depositions involving delicate, thermally sensitive substrates, such as those used in the processing of semiconductor components, physical vapor deposition (PVD) techniques[15] are employed. Such PVD techniques include sputter deposition,[16] reactive ion platting,[17] and arc deposition or evaporation techniques.[18] Zirconium nitride powders are synthesized by carbothermal reduction

† Department of Chemistry.
‡ Institute of Materials Science.
* To whom correspondence should be addressed.

(1) Oestling, M.; Nygren, S.; Petersson, C. S. *Thin Solid Films* **1986**, *145*, 81.
(2) (a) Rochotzki, R.; Vetter, J.; Weissmantel, E. *Thin Solid Films* **1991**, *198*, 103. (b) Vetter, J.; Rochotzki, R. *Thin Solid Films* **1990**, *192*, 253. (c) Jindal, P. C.; Quinto, D. T. *Surf. Coat. Technol.* **1988**, *36*, 683. (d) Fenske, G. R.; Kaufhen, N.; Lee, R. H.; Kremer, B. M.; Bunshah, R. F.; Sproul, W. D. *Surf. Coat. Technol.* **1988**, *36*, 791. (e) Sproul, W. D. *AIP Conf. Proc.* **1986**, *149*, *Phys. Chem. Prot. Coat. 157*. (f) Munz, W.-D. *J. Vac. Sci. Technol. A* **1986**, *4*, 2717. (g) Molarius, J. M.; Korhonen, A. S.; Harju, E.; Lappalainen, R. *Surf. Coat. Technol.* **1987**, *33*, 117.
(3) Sue, J. A.; Troue, H. H. *Surf. Coat. Technol.* **1991**, *49*, 31.
(4) (a) Wiiala, U. K.; Penttinen, I. M.; Korhonen, A. S.; Aromaa, J.; Ristolainen, E. *Surf. Coat. Technol.* **1990**, *41*, 191. (b) Harju, E. J.; Penttinen, J. M.; Korhonan, A. S.; Lappalainen, R. *Surf. Coat. Technol.* **1990**, *41*, 157. (c) Tari, M.; Forsen, O.; Aromaa, J. *Mater. Sci. Forum.* **1989**, *44* (*Electrochem. Methods Corros. Res.*) 15.
(5) (a) Tanabe, K.; Asano, H.; Katoh, Y.; Michikami, O. *Jpn. J. Appl. Phys. Pt. 2* **1987**, *26*, L570. (b) Geerk, J.; Linker, G.; Smithey, R. *Phys. Rev. Lett.* **1986**, *57*, 3284. (c) Schwartz, K.; Yee, D. S.; Cuomo, J. J.; Harper, J. M. E. *Phys. Rev. B: Condens. Matter* **1985**, *32*, 5419.
(6) Molarius, J. M.; Korhonen, A. S.; Harju, E.; Lappalainen, R. *Surf. Coat. Technol.* **1987**, *33*, 117.
(7) (a) Randhawa, H. *Surf. Coat. Technol.* **1988**, *36*, 829. (b) Koenig, U. *Surf. Coat. Technol.* **1987**, *33*, 91.
(8) (a) Bonnot, A. M.; Belkhir, H.; Pailharey, D.; Marthiez, P. *Sol. Energy Mater.* **1986**, *14*, 375. (b) Liu, J. S.; Ignatiev, A. *Sol. Energy Mater.* **1986**, *13*, 399.
(9) (a) Haygarth, J. C. *Thin Solid Films* **1980**, *72*, 51. (b) Karlsson, B.; Ribbing, C. G. *SPIE, Optical Coatings for Energy Efficiency and Solar Applications* **1982**, *324*, 52.
(10) (a) Oestling, M.; Nygren, S.; Petersson, C. S.; Norstroem, H.; Buchta, R.; Blom, H. O.; Berg, S. *Surf. Coat. Technol.* **1986**, *145*, 81. (b) Oestling, M.; Nygren, S.; Petersson, C. S.; Norstroem, H.; Wiklund, P.; Blom, H. O.; Berg, S. *J. Vac. Sci. Technol. A* **1984**, *2*, 281. (c) Krusin-Elbaum, L.; Wittmer, M.; Ting, C.-Y.; Cuomo, J. J. *Thin Solid Films* **1983**, *104*, 81.
(11) (a) Meng, W. J.; Morelli, D. T.; Roessler, D. M.; Heremans, J. *J. Appl. Phys.* **1991**, *69*, 846. (b) Marksteiner, P.; Weinberger, P.; Neckel, A.; Zelker, R.; Dedericks, P. H. *J. Phys. F: Met. Phys.* **1986**, *16*, 1495. (c) Saib, M.; Francois, J. C.; Gravier, P.; Sigrist, M.; Argeme, L.; Cerclier, O. *Solid State Commun.* **1986**, *58*, 385. (d) Izumi, K.; Masonobu D.; Ariyoshi, H. IEEE Trans. on Parts, Hybrids and Packaging **1975**, *PHP-11*, 105. (e) Josephson junctions: Schwartz, K.; Williams, A. R.; Cuomo, J. J.; Harper, J. M. E. *Phys. Rev B Condens. Matter* **1985**, *32*, 8312.
(12) Yotsuya, T.; Yoshitake, M.; Yamamoto, J. *Appl. Phys. Lett.* **1987**, *51*, 235.
(13) (a) Wittmer, M.; Studer, B.; Melchior, H. *J. Appl. Phys.* **1981**, *52*, 5722. (b) Wittmer, M. *J. Vac. Sci. Technol.* **1985**, *3*, 1797.
(14) (a) Wendel, H.; Surh, H. *Appl. Phys. A* **1992**, *A54*, 389. (b) Fix, R.; Gordon, R. G.; Hoffman, D. M. *Chem. Mat.* **1991**, *3*, 1138. (c) Schlegel, A.; Wachter, P.; Nickl, J. J.; Lingg, H. J. *J. Phys. C: Solid State Phys.* **1977**, *10*, 4889. (d) Karlsson, B.; Shimshock, R. P.; Seraphin, B. O.; Haygarth, J. C. *Solar Energy Mater.* **1983**, *7*, 401.

0897-4756/94/2806-0918$04.50/0

and nitridation.[19] This involves intimate mixing of zirconium oxide with a source of carbon, and heating to above 1300 °C in a nitrogen-containing atmosphere. The most common source of carbon is elemental carbon. However, this method still leaves residual carbon in the zirconium nitride product and requires a second oxidation step to remove the residual carbon. Moreover, it requires a temperature of at least 1300 °C. As with any synthesis process, it is desirable to keep energy consumption as low as possible. Therefore, an improved method of making zirconium nitride powder at a relatively lower temperature is desired in industry. This paper addresses an alternative method for the synthesis of zirconium nitride powder at a reaction temperature lower than 1300 °C, using methane as a reducing agent in the nitridation of zirconia.

An initial step in determining the process conditions, e.g., reagent concentrations, temperature, and pressure, which would lead to the conversion of ZrO_2 to ZrN is to perform thermodynamic calculations. A conversion diagram can then be constructed for the reaction system so that the positions of the phase boundaries can be accurately determined. The thermodynamic calculations also give the conversion efficiencies for the solid phase, namely, zirconium oxide, as well as the reactant gases, ammonia and methane.

Experimental Section

Thermodynamic Calculations. Several reactions for forming ZrN from ZrO_2 were first considered. A calculation for the temperature range between 600 and 2000 K was carried out based solely on free energy changes for these reactions:

$$2ZrO_2(s) + 4C(s) + 2N_2(g) \rightarrow 2ZrN(s) + 4CO(g) \quad (1)$$

$$2ZrO_2(s) + 4C(s) + 2NH_3(g) \rightarrow 2ZrN(s) + 3H_2(g) + 4CO(g) \quad (2)$$

$$2ZrO_2(s) + 4CH_4(g) + 2N_2(g) \rightarrow 2ZrN(s) + 8H_2(g) + 4CO(g) \quad (3)$$

$$2ZrO_2(s) + 4CH_4(s) + 2NH_3(g) \rightarrow 2ZrN(s) + 11H_2(g) + 4CO(g) \quad (4)$$

The changes in free energy for these systems were solved graphically (Figure 1), and they represent straight-line equations. Free energy and temperature are variables, and the coefficients of the gradients of the straight lines are related to entropy. The most feasible reaction of the four considered is reaction 4 in which the net change in free energy obtained is negative at a temperature lower than those of the other three reactions as shown in Figure 1.

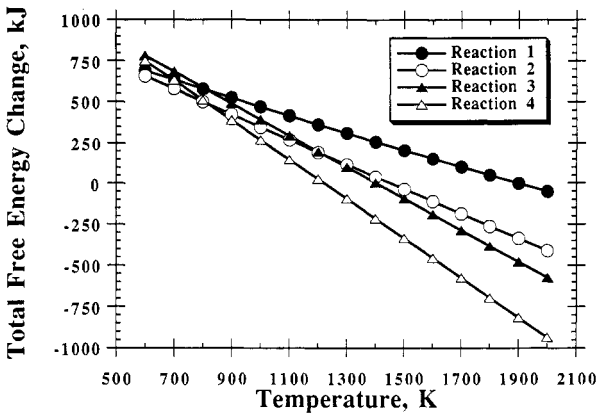

Figure 1. Gibbs free energy change of a few reactions 1–4 involving the conversion of aluminum oxide to aluminum nitride.

Since reaction 4 is the most feasible reaction for the conversion of zirconia to zirconium nitride, the thermodynamic calculations presented in this paper were performed for the Zr–N–C–H system. NH_3 was selected as it is inexpensive, readily available, a reactive nitrogen source, and can significantly reduce the reaction temperature.[14c,d,20] CH_4 was selected as the readily available reducing agent.

Computerized thermodynamic calculations were carried out using the SOLGASMIX-PV program,[21] which is a modified version of the SOLGASMIX program.[22] Table 1 lists the thermodynamic data at 1600, 1800, and 2000 K for the possible gaseous, liquid, and solid species for the NH_3–ZrO_2–CH_4 system. The thermodynamic data for the various species were taken from the JANAF tables.[23] The calculations predict the equilibrium composition of the solid–gas system based on the minimization of the free energy of all the possible gaseous, liquid, and solid species. Numerous chemical equilibrium thermodynamic analyses of this type have already proven useful in understanding chemical processes.[24–27]

The calculations conducted in this study were performed for combinations of ZrO_2 + NH_3 + CH_4 over the range 0–100 mol % concentrations of the reagents. Reagent compositions were varied by 5 mol % increments. The positions of the phase boundaries were more precisely determined by subsequent calculations using 1 mol % increments. Calculations were performed to determine the effects of temperature, total gas pressure, and addition of hydrogen on the thermodynamic predictions of the NH_3–ZrO_2–CH_4 system.

Synthesis and Characterization of Zirconium Nitride Powder. ZrO_2 powder was prepared by a sol–gel technique. Zirconyl nitrate (Aldrich, 0.1 mol) was dissolved in 100 mL of water. Ammonium hydroxide was then added dropwise to the zirconyl nitrate solution, with constant stirring, until the solution reached a pH of 9. The resulting sol–gel was centrifuged, and the gel was washed twice with doubly deionized water. The washed gel was then dried in an oven at 110 °C for 12 h. The powder obtained was fired at 1000 °C in air for 12 h to convert it to ZrO_2.

For the nitridation step, anhydrous ammonia (zero grade, Aero All Gas Co.) was used as the nitrogen source and methane (zero grade, Aero All Gas Co.) was used as the reducing agent. The two gases were mixed upstream of the reactor. Figure 2 is a schematic of the apparatus used to synthesize ZrN from the ZrO_2 powder obtained by the method described above. The reaction

(15) (a) Fillit, R. Y.; Perry, A. J.; Strandberg, C. *Thin Solid Films* **1991**, *197*, 47. (b) Rochotzki, R.; Vetter, J.; Weissmantel, E. *Thin Solid Films* **1991**, *198*, 103. (c) Vetter, J.; Rochotzki, R. *Thin Solid Films* **1990**, *192*, 253. (d) Wiiala, U. K.; Penttinen, I. M.; Korhonen, A. S.; Aromaa, J.; Ristolainen, E. *Surf. Coat. Technol.* **1990**, *41*, 191. (e) Quinto, D. T.; Wolfe, G. J.; Jindal, P. C. *Thin Solid Films* **1987**, *153*, 19.

(16) (a) Sell, J. A.; Meng, W. J.; Perry, T. A. *J. Vac. Sci. Technol. A, Part 2* **1992**, *10*, 1804. (b) Meng, W. J.; Sell, J. A.; Waldo, R. A. *J. Vac. Sci. Technol. A* **1991**, *9*, 2183. (c) Yoshitake, M.; Yotsuya, T.; Takiguchi, K.; Ogawa, S. *Jpn. J. Appl. Phys., Part 1* **1990**, *29*, 2800. (d) Netterfield, R. P.; Martin, P. J.; McKenzie, D. R. *J. Mater. Sci. Lett.* **1990**, *9*, 972. (e) Sproul, W. D. *J. Vac. Sci. Technol. A* **1986**, *4*, 2874. (f) Sproul, W. D. *Thin Solid Films* **1983**, *107*, 141. (g) Yoshitake, M.; Takiguchi, K.; Suzuki, Y.; Ogawa, S. *J. Vac. Sci. Technol.* **1988**, *6*, 2326.

(17) (a) Molarius, J. M. *Sci. Tech. Aerosp. Rep.* **1988**, *26*, ETN-88-92218; N88-22167. (b) Salmenoja, K.; Korhonen, A. S. *Vacuum* **1986**, *36*, 33. (c) Salmenoja, K.; Korhonen, A. S.; Erola, E.; Molarius, J. M. *Appl. Phys. Lett.* **1986**, *49*, 1986.

(18) Johnson, P. C.; Randhawa, H. *Surf. Coat. Technol.* **1987**, *33*, 53.

(19) (a) Somiya, S.; Suzuki, K.; Yoshimura, M. *Horiz. Powder Metall., Proc. Int. Powder Metall. Conf. Exhib.* **1986**, *1*, 179. (b) Somiya, S.; Suzuki, K.; Yoshimura, M. *Adv. Ceram.* **1987**, *21*, 279. (c) Hirao, K.; Miyamoto, Y.; Koizumi, M. *Adv. Ceram.* **1987**, *21*, 289. (d) Brown, G. M.; Maya, L. *J. Am. Ceram. Soc.* **1988**, *71*, 78.

(20) Kurtz, S. R.; Gordon, R. G. *Thin Solid Films* **1986**, *140*, 277.

(21) Besmann, T. M. *ORNL/TM-5775*, Oak Ridge National Laboratory, Oak Ridge, TN, Apr 1977.

(22) Eriksson, G. *Chem. Scr.* **1975**, *8*, 100.

(23) JANAF Thermochemical Tables, 3rd ed., Parts I and II; *J. Phys. Chem. Ref. Data*, Supplement No. 1 **1985**, *14*.

(24) Fischman, G. S.; Petuskey, W. T. *J. Am. Ceram. Soc.* **1985**, *68*, 185.

(25) Kingon, A. I.; Lutz, L. J.; Davis, R. F. *J. Am. Ceram. Soc.* **1983**, *66*, 551.

(26) Besmann, T. M. *J. Am. Ceram. Soc.* **1986**, *69*, 69.

(27) Kingon, A. I.; Lutz, L. J.; Liaw, P.; Davis, R. F. *J. Am. Ceram. Soc.* **1983**, *66*, 558.

Table 1. Enthalpy and Entropy Data at 1600, 1800, and 2000 K Used in the SOLGASMIX-PV Calculations

	1600 K		1800 K		2000 K	
species	$\Delta H_f°$, kJ/mol	$S_f°$, J/(mol K)	$\Delta H_f°$, kJ/mol	$S_f°$, J/(mol K)	$\Delta H_f°$, kJ/mol	$S_f°$, J/(mol K)
Zr(g)	601.919	-225.457	601.556	-228.944	601.000	-232.163
ZrN(g)	697.932	-292.892	695.626	-297.320	692.923	-301.294
ZrO(g)	48.556	-291.882	49.011	-295.035	49.096	-303.565
ZrO_2(g)	-300.518	-363.509	-302.714	-370.280	-305.358	-376.352
H_2N(g)	184.066	-260.827	183.925	-266.728	183.891	-272.168
H_3N(g)	-55.847	-275.788	-55.439	-283.962	-54.833	-291.525
N_3(g)	421.865	-313.082	423.252	-320.148	424.602	-326.515
CO(g)	-115.933	-250.707	-117.384	-245.912	-118.896	-258.714
C_1(g)	718.092	-193.053	717.373	-195.509	716.577	-197.713
C_2(g)	834.465	-262.287	832.266	-266.750	830.000	-270.801
C_3(g)	799.940	-307.534	795.226	-313.394	790.421	-318.731
C_4(g)	963.358	-344.056	960.404	-353.832	957.248	-362.660
CH(g)	590.972	-235.698	590.329	-240.149	589.723	-244.238
CH_2(g)	378.809	-264.073	377.835	-270.280	376.844	-275.953
CH_3(g)	134.262	-281.768	133.554	-290.082	132.917	-297.727
CH_4(g)	-92.703	-285.413	-92.797	-296.039	-92.709	-305.853
C_2H(g)	470.010	-285.807	468.346	-292.535	466.681	-298.689
C_2H_2(g)	181.619	-303.546	174.353	-312.829	166.980	-321.335
C_2H_4(g)	35.249	-394.044	35.005	-362.460	34.894	-374.791
C_3O_2(g)	-93.313	-424.225	-94.192	-436.706	-95.209	-447.989
C_2O(g)	285.161	-321.704	284.143	-329.043	283.063	-335.695
CO_2(g)	-395.876	-295.983	-396.311	-302.968	-396.784	-309.293
H(g)	225.289	-149.640	226.132	-152.088	226.898	-154.278
H_2(g)	0.000	-180.944	0.000	-171.790	0.000	-188.418
C_5(g)	972.041	-388.560	968.885	-401.096	965.493	-412.421
N(g)	478.791	-188.224	497.411	-190.672	479.990	-192.863
N_2(g)	0.000	-244.138	0.000	-248.304	0.000	-252.074
NO(g)	90.525	-265.019	90.522	-269.282	90.494	-273.128
NO_2(g)	32.724	-319.288	32.940	-325.861	33.111	-331.788
NO_3(g)	77.925	-366.807	79.411	-376.308	80.809	-384.856
N_2O(g)	86.432	-303.608	87.488	-310.577	88.527	-216.871
N_2O_3(g)	91.079	-451.187	92.854	-462.941	94.557	-473.537
N_2O_4(g)	25.922	-483.167	29.550	-498.193	33.110	-511.743
N_2O_5(g)	34.706	-562.877	38.487	-580.176	42.064	-595.711
NH(g)	376.438	-232.465	376.488	-236.528	376.551	-240.233
N_2H_2(g)	207.649	-308.365	208.504	-316.936	209.457	-324.781
N_2H_4(g)	92.401	-377.067	94.871	-390.490	97.538	-402.810
O(g)	254.421	-196.599	254.884	-199.053	255.299	-201.247
O_2(g)	0.000	-260.434	0.000	-264.796	0.000	-268.748
O_3(g)	144.987	-323.551	145.419	-330.349	145.784	-336.469
N_2C_4(g)	538.791	-473.793	538.075	-489.052	537.186	-502.844
NC(g)	257.093	-256.046	251.791	-260.333	246.516	-264.251
CNO(g)	160.353	-317.683	160.165	-324.715	159.895	-331.057
CN_2(g)	585.397	-316.474	585.113	-323.351	584.786	-329.573
H_2O(g)	-250.592	-253.690	-251.138	-259.451	-251.575	-264.769
Zr(l)	16.307	-96.826	18.388	-101.754	20.089	-106.163
ZrC(l)	-118.780	-136.694	-118.688	-143.329	-118.926	-149.338
ZrN(l)	-286.017	-145.579	-284.213	-152.426	-282.539	-158.704
ZrO_2(l)	-1007.613	-197.325	-1006.412	-206.097	-1005.687	-213.944
Zr(s)	0.000	-89.511	0.000	-93.211	0.000	-96.722
ZrC(s)	-196.556	-116.422	-196.464	-123.057	-196.702	-129.066
ZrN(s)	-360.532	-122.099	-358.727	-128.945	-357.054	-135.223
ZrO_2(s)	-1081.921	-173.028	-1080.720	-181.800	-1079.995	-189.647
C(s)	0.000	-35.270	0.000	-38.149	0.000	-40.771

takes place in a quartz tube reactor. About 0.1 g of ZrO_2 powder was placed in a quartz boat and placed into the reactor, which was then positioned in the furnace and heated in He to the reaction temperature of 1100 °C at a rate of 11.5 °C/min. Once the ZrO_2 reached the reaction temperature, the gaseous reactant mixture was flowed into the reactor. The flow rates for ammonia and methane were kept at 400 and 11 mL/min, respectively, providing an NH_3/CH_4 molar ratio of 36.7. The reaction conditions were maintained for 3 h to obtain the desired conversion into ZrN. After this time, the gaseous reactant mixture was shut off and He was flowed into the reactor so that a nonreactive atmosphere was established in the reactor. The reactor and product were then cooled to room temperature.

Powder X-ray diffraction data of the product were obtained using a Scintag XDS 2000 Theta-theta diffractometer. Monochromated Cu Kα radiation was used and a scan rate of 2 degree per minute and a step size of 0.03 degrees were employed. The Kα_2 component was stripped by the Rachinger method.[28] Peak positions were calibrated by using a quartz standard.

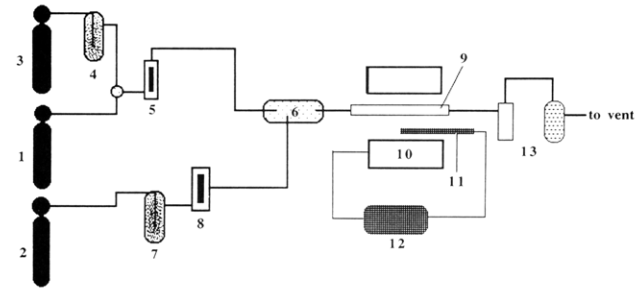

Figure 2. Schematic of the reactor system used for the synthesis of ZrN from sol-gel ZrO_2 powder: (1) helium gas; (2) ammonia gas; (3) methane gas; (4) molecular sieve; (5) flow meter; (6) gas mixing chamber; (7) molecular sieve; (8) flow meter; (9) quartz reactor; (10) furnace; (11) temperature probe; (12) temperature controller; (13) gas scrubbers.

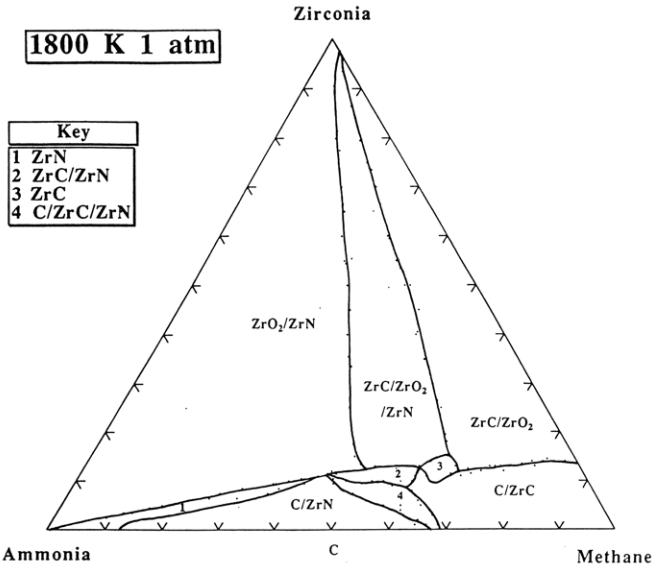

Figure 3. Conversion diagram for the reactant system ZrO_2(s)-CH_4(g)-NH_3(g) at 1800 K and 1.0 atm pressure showing the region where it is predicted, from thermodynamic considerations alone, that pure ZrN phase may be formed.

Results and Discussion

Conversion/Phase Diagrams. Conversion diagrams, such as the one shown in Figure 3, can be constructed from the results of the thermodynamic calculations. These diagrams show the equilibrium solid phase(s) as a function of reagent concentrations for a specific temperature and total gas pressure for the reagent system NH_3-ZrO_2-CH_4. The conversion diagram in Figure 3 is for a temperature of 1800 K and 1 atm total gas pressure (P_{tot} = 1 atm). Thermodynamic calculations predict three relatively large regions, namely, ZrO_2/ZrN, ZrC/ZrO_2/ZrN, and ZrC/ZrO_2. These regions represent incomplete conversion of ZrO_2 into ZrN and/or ZrC. At the base of the triangle, where the mole ratio of ZrO_2 is low, regions of C/ZrN, C/ZrC/ZrN and C/ZrC exist. In these regions, complete conversion of ZrO_2 into ZrN and/or ZrC occurs with codeposition of carbon from thermal decomposition/oxidation of methane. At higher mole ratios of ZrO_2, no deposition of C occurs giving rise to regions 2 (ZrC/ZrN) and 3 (ZrC).

The region of particular interest is region 1. Within this area, conversion of ZrO_2 to ZrN proceeds to completion and pure ZrN is formed. Reagent composition for this one-phase region includes a high molar ratio of NH_3 (>60

(28) Rachinger, W. A. *J. Sci. Instrum.* **1948**, *25*, 254.

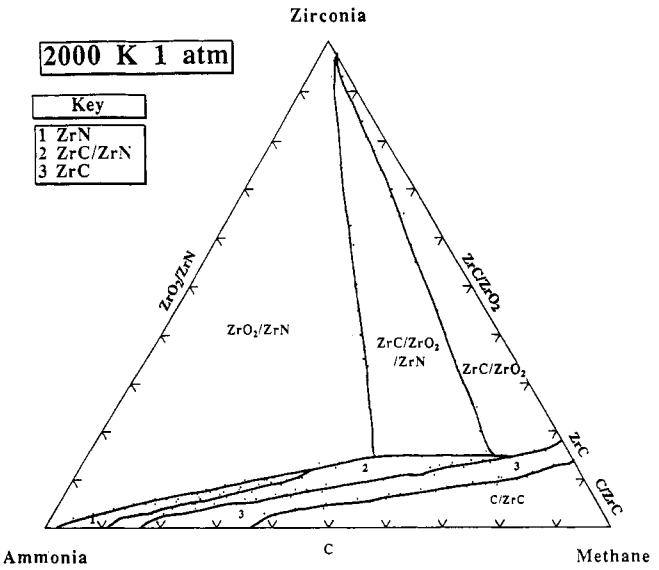

Figure 4. Conversion diagram obtained at higher temperature (2000 K, 1.0 atm pressure) shifts the area of the pure ZrN phase region toward lower mol % CH_4 and higher mol % NH_3.

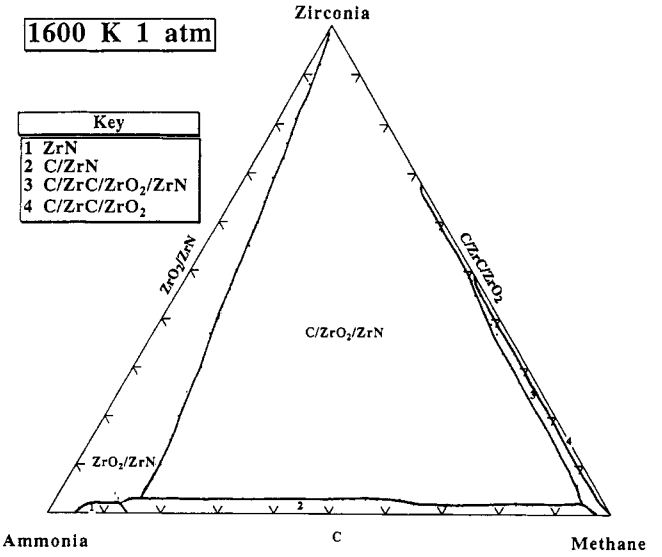

Figure 5. Thermodynamic considerations predict that at 1600 K and 1.0 atm pressure, the region in which pure ZrN is formed is very much reduced in area.

mol %) and low molar ratio of ZrO_2 (<20 mol %). The amount of CH_4 has to be low in order to prevent coke formation.

At the corners of the triangle at 100 mol % NH_3 and 100 mol % CH_4, no solid phase is present. Only gases (NH_3 and CH_4, respectively) are present at equilibrium. At 100 mol % ZrO_2, the only solid phase present is ZrO_2. No gases are present at equilibrium. For the line joining the two corners of 100 mol % NH_3 and 100 mol % CH_4, the only solid phase present is C. Two solid phases are predicted, namely, ZrN and ZrO_2, along the line joining 100 mol % ZrO_2 and 100 mol % NH_3. It is predicted that two phases (ZrO_2 + ZrC) exist at equilibrium along the line joining 100 mol % CH_4 and 100 mol % ZrO_2 when the mole % ZrO_2 is higher than 15 mol %. Below 15 mol % ZrO_2, a mixed C/ZrC phase is formed.

To determine the effect of reaction conditions such as temperature, total system pressure and hydrogen concentration on the conversion of ZrO_2 to ZrN, additional conversion diagrams were constructed. Several of those diagrams are presented in this paper to illustrate the effects of changes in the conversion process.

The influence of higher temperature (2000 K) at P_{tot} = 1 atm results in the single, pure ZrN-phase region being shifted toward lower mol % CH_4 but higher mol % NH_3. This is shown by the conversion diagram in Figure 4. Other changes are also observed at higher reaction temperatures. For example, the C/ZrC/ZrN and C/ZrN phase regions, observed at 1800 K, are not present at 2000 K. Instead the ZrC/ZrN, ZrC, and C/ZrC regions extend in area, covering the major portion of the base of the conversion diagram. In addition, the ZrO_2/ZrN and ZrC/ZrO_2/ZrN phase regions expand in area at the expense of the ZrC/ZrO_2 phase region. As shown in Figure 5, decreasing the reaction temperature to 1600 K, on the other hand, significantly reduces the area of the single pure ZrN phase region. Pure ZrN can only be formed at NH_3 concentrations greater than 85 mol %. The C/ZrO_2/ZrN phase region accounts for the major part of the conversion diagram. Carbon deposition dominates the conversion diagram, making synthesis of ZrN at low temperatures undesirable. Low temperatures also result in C/ZrC/ZrO_2 being formed along the line joining 100 mol % ZrO_2 and 100 mol % CH_4.

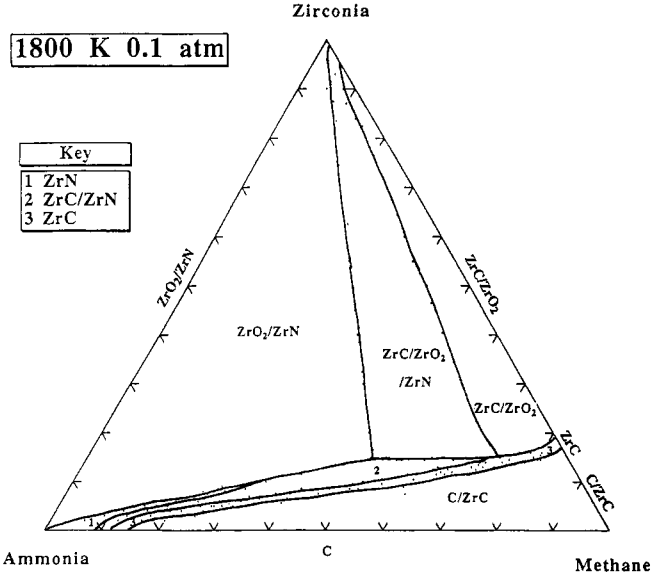

Figure 6. Decreasing the total system pressure to 0.1 atm while maintaining the temperature at 1800 K results in a drastic decrease in the area of the pure ZrN phase region accompanied by an increase in areas of ZrC/ZrN, ZrC, and C/ZrC regions.

A decrease in pressure while maintaining the temperature at 1800 K also results in a drastic decrease in the area of the pure ZrN phase region (Figure 6). The ZrC/ZrN, ZrC, and C/ZrC regions increase in area and extend out to occupy the major part of the base of the conversion diagram. Comparing Figures 4 and 6 suggests that an increase in temperature (2000 K) or a decrease in pressure (P_{tot} = 0.1 atm) results in a similar, though not identical, conversion phase diagram.

Conversion Efficiencies. In this work, conversion efficiency is defined as the fraction of reagent that is converted to ZrN. For example, if 0.2 mol of ZrN is formed for every 1.0 mol of NH_3 introduced into the reaction system, the conversion efficiency of NH_3 into ZrN is 0.2. Similarly, we define deposition efficiency for CH_4 as the fraction of CH_4 that is deposited as solid graphite. A knowledge of C deposition efficiency will help in determining the experimental conditions that will not facilitate the deposition of C and hence eliminate the need to burn

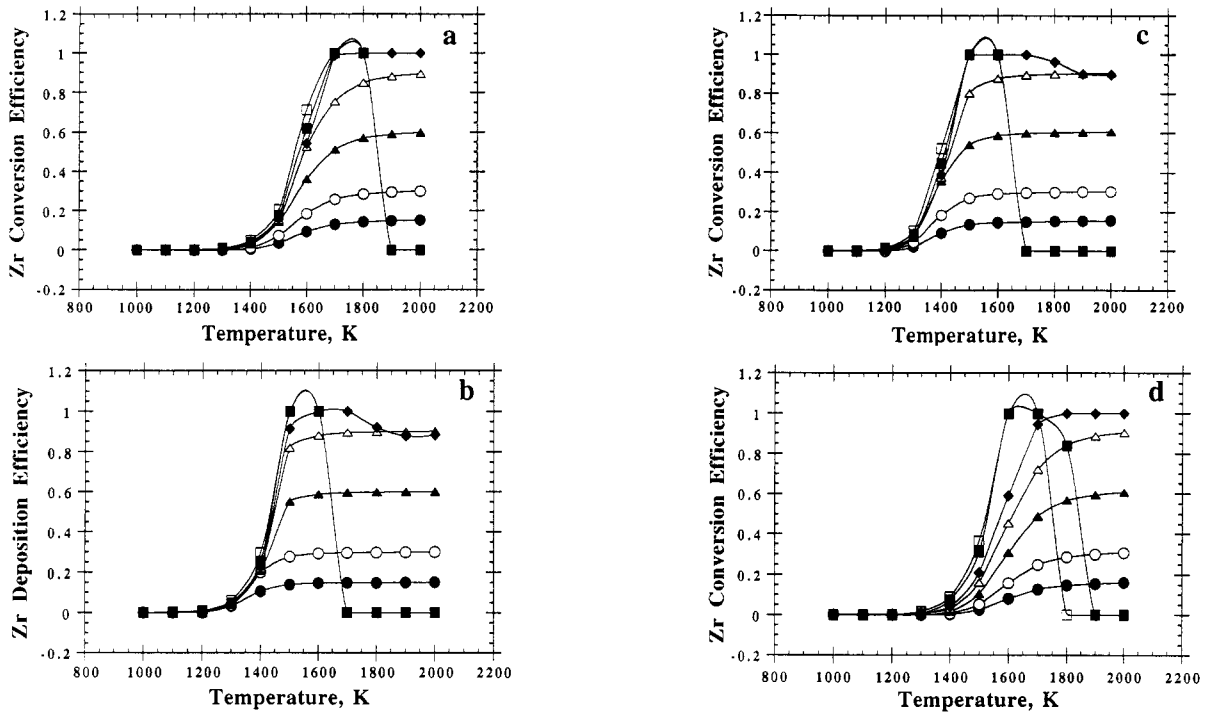

Figure 7. Zirconium conversion efficiency as a function of temperature for (a) P_{tot} = 1 atm, (b) P_{tot} = 0.1 atm; (c) P_{tot} = 0.1 atm and excess hydrogen (50 mol), and (d) P_{tot} = 1.0 atm and excess hydrogen (50 mol). The NH_3/ZrO_2 ratio was kept at 16. The Zr conversion efficiency increases with temperature until a maximum is reached around 1600 K. Each curve represents the conversion efficiency response of a specific CH_4/ZrO_2 ratio.

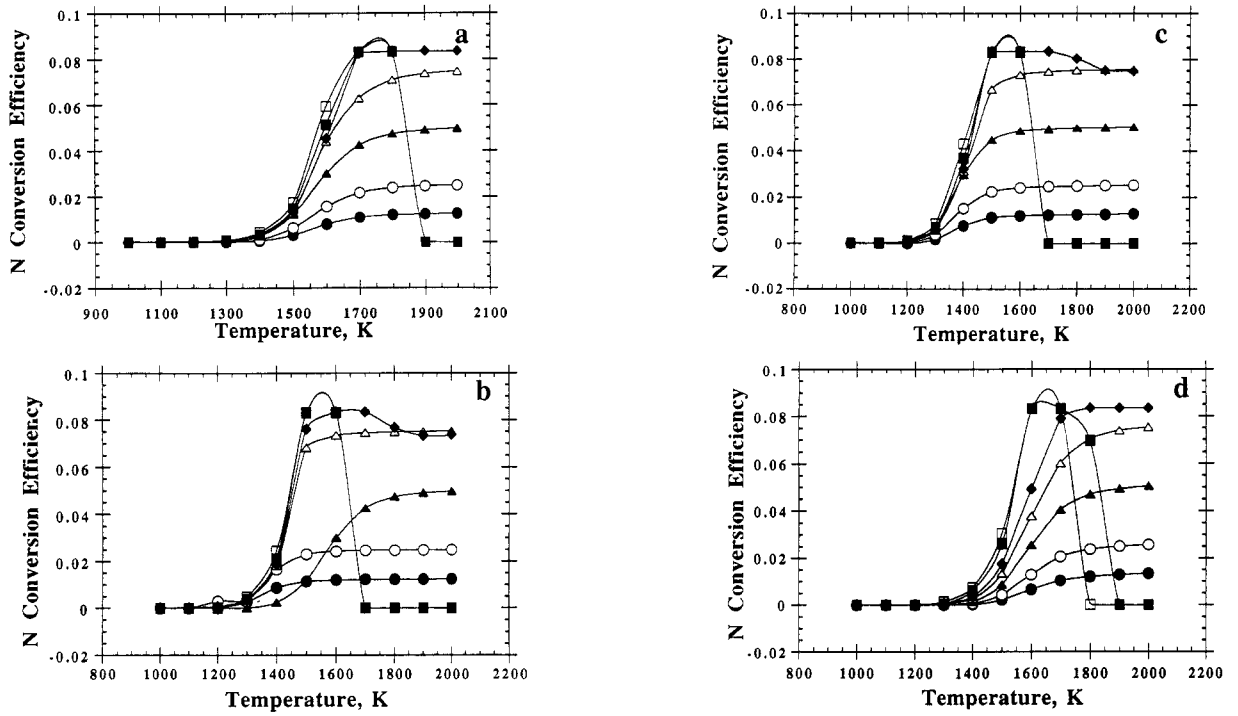

Figure 8. Nitrogen conversion efficiency as a function of temperature for (a) P_{tot} = 1 atm, (b) P_{tot} = 0.1 atm, (c) P_{tot} = 0.1 atm and excess hydrogen (50 mol), and (d) P_{tot} = 1.0 atm and excess hydrogen (50 mol). The NH_3/ZrO_2 ratio was kept at 16. The N conversion efficiency also increases with temperature until a maximum is reached around 1600 K. Each curve represents the conversion efficiency response of a specific CH_4/ZrO_2 ratio.

off the C deposited during the conversion process. Thermodynamic data at 1800 K were used in all calculations involving conversion/deposition efficiencies over the temperature range of interest (1000 K to 2000 K).

Figures 7 and 8 summarizes the conversion efficiency for Zr and N, respectively, over the temperature range 1000–2000 K. Since the results of the conversion diagrams suggest that a high mole fraction of ammonia favors the formation of pure ZrN, a high NH_3/ZrO_2 molar ratio is used in these calculations. The NH_3/ZrO_2 molar ratio is fixed at 16 and the plots were determined as a function of temperature. The effects of CH_4/ZrO_2 molar ratio (henceforth written as C/Zr), total system pressure, and the addition of hydrogen on the Zr–C–N system, as predicted by thermodynamic calculations alone, are examined. The shapes of the plots for Zr and N conversion

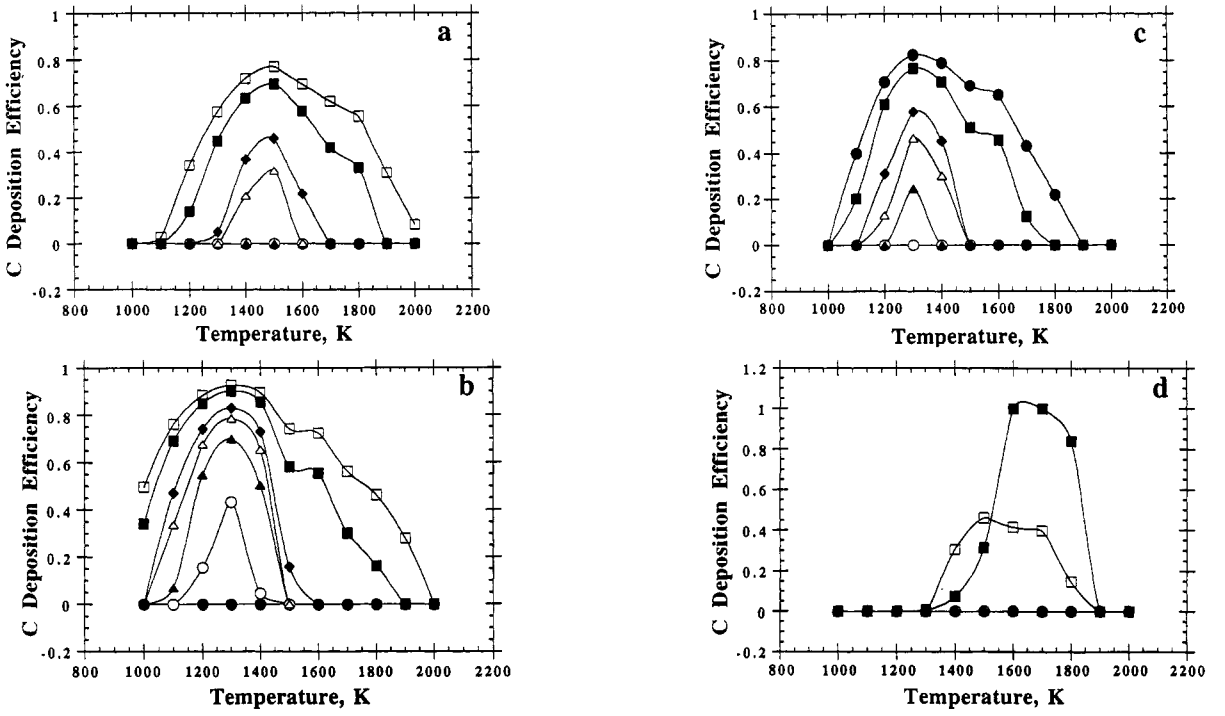

Figure 9. Carbon deposition efficiency as a function of temperature for (a) P_{tot} = 1 atm, (b) P_{tot} = 0.1 atm, (c) P_{tot} = 0.1 atm and excess hydrogen (50 mol), and (d) P_{tot} = 1.0 atm and excess hydrogen (50 mol). The NH_3/ZrO_2 ratio was kept at 16. The C deposition efficiency first increases with temperature until a maximum is reached and then decreases to zero. Each curve represents the conversion efficiency response of a specific CH_4/ZrO_2 ratio.

Table 2. Conversion/Deposition Efficiencies for Zirconium, Nitrogen, and Carbon as a Function of Methane to Zirconium Oxide and Ammonia to Zirconium Oxide Molar Ratios at 1800 K and Total System Pressure of 1.0 atm

	Zr conversion efficiency			N conversion efficiency			C deposition efficiency		
$CH_4:ZrO_2$ molar ratio	$NH_3:ZrO_2$ molar ratio			$NH_3:ZrO_2$ molar ratio			$NH_3:ZrO_2$ molar ratio		
	16	8	4	16	8	4	16	8	4
1	0.29	0.28	0.28	0.02	0.05	0.09	0.00	0.00	0.00
2	0.57	0.56	0.55	0.05	0.09	0.18	0.00	0.00	0.00
4	1.00	1.00	1.00	0.08	0.17	0.33	0.00	0.00	0.00
9	1.00	1.00	0.00	0.08	0.17	0.00	0.33	0.43	0.29

efficiencies are identical, but they differ in the conversion efficiency values for a particular temperature and CH_4/ZrO_2 molar ratio. With the exception of a C/Zr ≥ 9, the Zr and N conversion efficiencies increase to a maximum value and remain at that maximum value attained even at higher temperatures. In the case of a C/Zr ≥ 9, the conversion efficiency decreases to a value of zero at temperatures beyond the temperature which gives rise to the maximum conversion efficiency. At this point ZrC, rather than ZrN, is formed. An increase in C/Zr also causes an increase in the maximum attainable value for the Zr and N conversion efficiencies. For a fixed NH_3/ZrO_2 ratio, a change in the CH_4/ZrO_2 molar ratio does not significantly alter the Zr and N conversion efficiencies at low reaction temperatures but as the reaction temperature increases above 1400 K, an increase in CH_4/ZrO_2 molar ratio increases the Zr and N conversion efficiencies considerably.

Figure 9 summarizes the thermodynamic predictions for the C deposition efficiency for the same reactant molar ratios as those of Figures 7 and 8 and over the temperature range of 1000–2000 K. For P_{tot} = 1 atm, the C deposition efficiency increases initially to a maximum at about 1500 K for CH_4/ZrO_2 molar ratios greater than or equal to 2. No carbon deposition occurs at C/Zr ≤ 2.0. Above 1500 K, the C deposition efficiency then decreases to zero with increasing reaction temperature. At high temperatures, the C is consumed in the production of ZrC and gaseous C products, resulting in the absence of coke formation. An increase in C/Zr results in a greater C deposition efficiency for a given temperature. Thus, judging from the results of Figures 7–9, it is advantageous to employ a C/Zr of less than or equal to 4.0 and a reaction temperature of greater than or equal to 1700 K. Under these conditions, ZrN is formed with no C deposition, though it is not necessary that complete conversion of ZrO_2 into ZrN takes place. The ideal conditions, as predicted by thermodynamic calculations alone, would be a C/Zr = 4 and a reaction temperature between 1700 and 1800 K.

Table 2 summarizes conversion and deposition efficiencies for Zr, N, and C at 1800 K and P_{tot} = 1 atm as a function of CH_4/ZrO_2 and NH_3/ZrO_2 molar ratios. Increasing the C/Zr significantly increases the Zr conversion efficiencies for a given N/Zr ratio. On the other hand, keeping the C/Zr fixed while increasing the N/Zr does not increase the Zr conversion efficiency. This suggests that methane plays an important role in determining the extent of conversion of ZrO_2 to ZrN. Thermodynamic calculations predict that total conversion of ZrO_2 to ZrN occurs at C/Zr ≥ 4 when sufficient ammonia is present in the system. Insufficient ammonia results in the conversion of ZrO_2 to ZrC, as shown by the data for C/Zr = 9 and N/Zr = 4.

N conversion efficiency follows a similar trend. For a given N/Zr, the N conversion efficiency increases with increase in C/Zr. However, the N conversion efficiency

decreases with increase in N/Zr while the C/Zr was kept constant. This suggests that at high NH_3/ZrO_2 molar ratios, ZrO_2 is the limiting reactant with excess ammonia being converted into gaseous nitrogenous products. Alternatively, the excess ammonia passes through the system without being converted into another nitrogen containing compound at all.

Table 2 also indicates that for C/Zr ≤ 4, conversion of ZrO_2 to ZrN occurs without C deposition at 1800 K even at N/Zr = 4. In fact, complete conversion of ZrO_2 into ZrN is feasible without C deposition for C/Zr = 4. However, C deposition occurs at C/Zr ≥ 9. Thus, even though complete conversion of ZrO_2 to ZrN is still possible at C/Zr = 8, the co-deposition of carbon makes nitridation of ZrO_2 at high C/Zr ratios (C/Zr ≥ 9) unfavorable.

Effect of Low Pressure and Excess Hydrogen on Zr and N Conversion Efficiencies. Figures 7 and 8 also compare the effects of low pressure and hydrogen addition on the Zr and N conversion efficiency, respectively. The N/Zr molar ratio is kept at 16. Figures 7b and 8b suggest that decreasing P_{tot} from 1.0 to 0.1 atm results in a shift toward lower temperatures at which maximum Zr and N conversion efficiencies are obtained. However, a decrease in P_{tot} does not result in any significant change in the maximum attainable Zr and N conversion efficiencies. Another difference observed at P_{tot} = 0.1 atm is the decrease in conversion efficiencies at temperatures above 1800 K for C/Zr ≥ 4. With the exception of C/Zr = 4, addition of excess hydrogen (50 mol) at P_{tot} = 0.1 atm (Figures 7c and 8c) does not change the shape of the Zr and N conversion efficiency plots from those at P_{tot} = 0.1 atm (without excess hydrogen). In the case where C/Zr = 4, the presence of hydrogen results in a slower decline of the conversion efficiencies for temperatures greater than 1800 K. Addition of excess hydrogen at P_{tot} = 1.0 atm also slows down the decline of the conversion efficiencies for C/Zr ≥ 9 at high temperatures (≥1800 K).

Thus a decrease in total system pressure encourages the formation of ZrC at high temperatures (>1800 K) and high C/Zr ratios (C/Zr > 4), resulting in a decrease in Zr and N conversion efficiencies. On the other hand, the addition of hydrogen into the system discourages the formation of ZrC and thus slows down the decline in conversion efficiencies under these reaction conditions.

Another way to to analyze the results of Figures 7 and 8 is to consider the conversion/deposition efficiency *ratio*. The conversion/deposition efficiency ratio for a specific temperature is defined as the ratio of the conversion efficiency for a particular set of conditions (pressure and/or introduction of excess hydrogen) to the conversion/deposition efficiency obtained at 1.0 atm pressure at that temperature with no excess hydrogen introduced into the system. Since Figures 7 and 8 predict that ZrN is formed at temperatures of at least 1400 K, conversion/deposition efficiency ratios are plotted from 1400 through 2000 K.

For a total system pressure of 0.1 atm (P_{tot} = 0.1 atm), a general trend observed is that the Zr and N conversion efficiency ratios are higher than 1.0 for temperatures lower than 1600 K for all C/Zr ratios. In other words, there is greater conversion of ammonia and zirconium oxide into zirconium nitride at P_{tot} = 0.1 atm than at P_{tot} = 1.0 atm. This is true even with the introduction of excess hydrogen (50 moles) into the system. Although Zr and N conversion efficiencies are higher at these conditions, the absolute conversion efficiency values are low and a large fraction

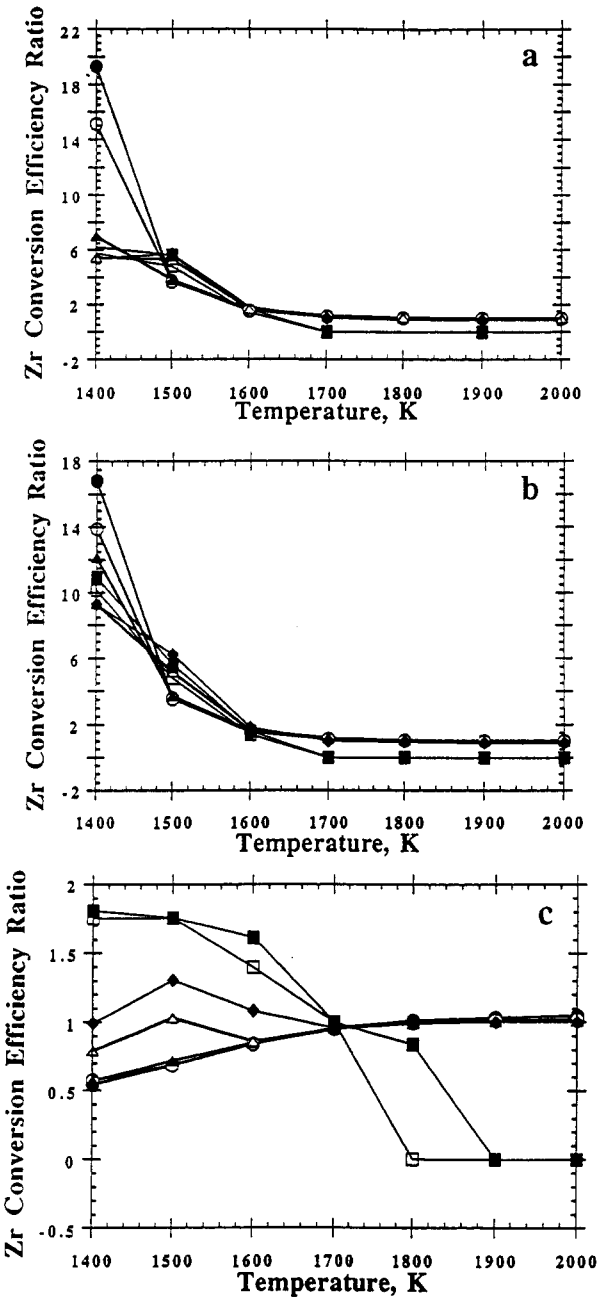

Figure 10. Effects of (a) low pressure (0.1 atm), (b) a combination of low pressure (P_{tot} = 0.1 atm) and excess hydrogen (50 mol), and (c) addition of excess hydrogen (50 mol, P_{tot} = 1 atm) on the Zr conversion efficiency ratio. The NH_3/ZrO_2 ratio was kept at 16. Each curve represents the conversion efficiency ratio response for a specific CH_4/ZrO_2 ratio as indicated in the figure. Note the differences in the *y* axis scale for each figure.

of ZrO_2 still remains unconverted to ZrN (see Figures 7 and 8). Greater conversion efficiency ratios are not observed in the system where there is excess hydrogen at P_{tot} = 1.0 atm. In this system, N and Zr conversion efficiency ratios are less than 1.0 for C/Zr < 4, equal to 1.0 for C/Zr = 4, and greater than 1.0 for C/Zr > 4.

Above 1600 K, Zr and N conversion efficiency ratios decrease to 1.0 for C/Zr ≤ 4 and P_{tot} = 0.1 atm (with or without excess hydrogen present). For C/Zr > 4, the conversion efficiency ratios fall to zero because ZrC, rather than ZrN, is formed. Thus at high temperatures (>1600 K), decreasing the pressure and/or introducing excess hydrogen into the system does not increase the conversion efficiencies. Comparison of Figures 10 and 11 reveals that

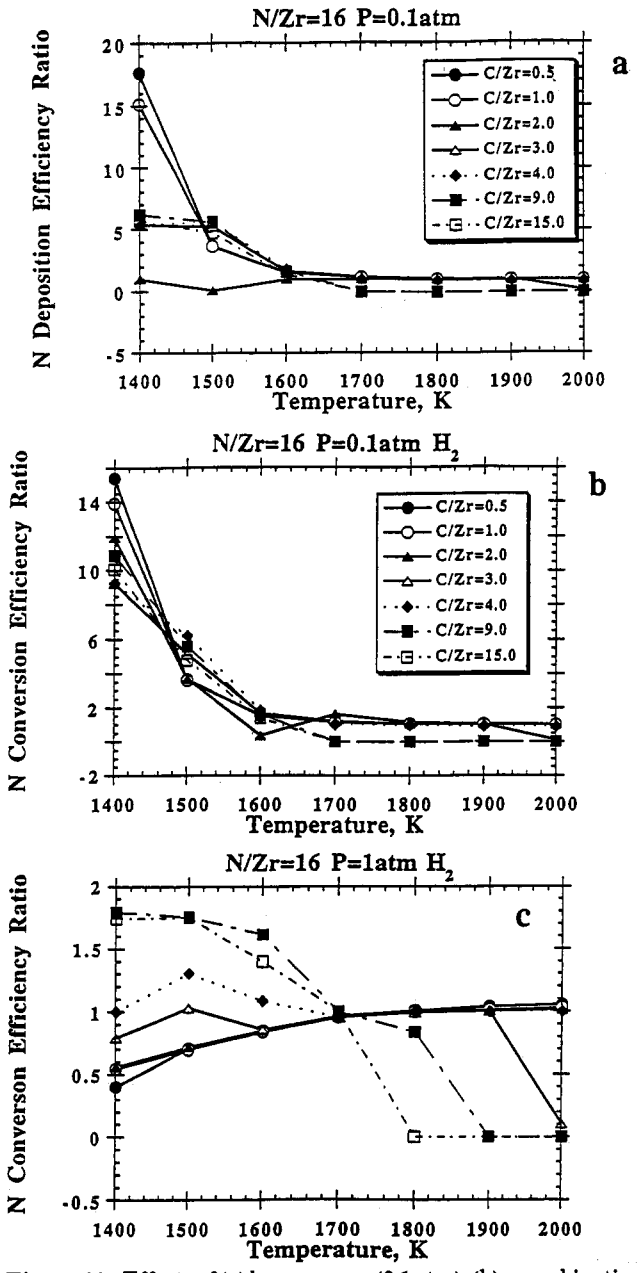

Figure 11. Effects of (a) low pressure (0.1 atm), (b) a combination of low pressure (P_{tot} = 0.1 atm) and excess hydrogen (50 mol), and (c) addition of excess hydrogen (50 mol, P_{tot} = 1 atm) on the N conversion efficiency ratio. The NH_3/ZrO_2 ratio was kept at 16. Each curve represents the conversion efficiency ratio response for a specific CH_4/ZrO_2 ratio as indicated in the figure. Note the differences in the y axis scale for each figure.

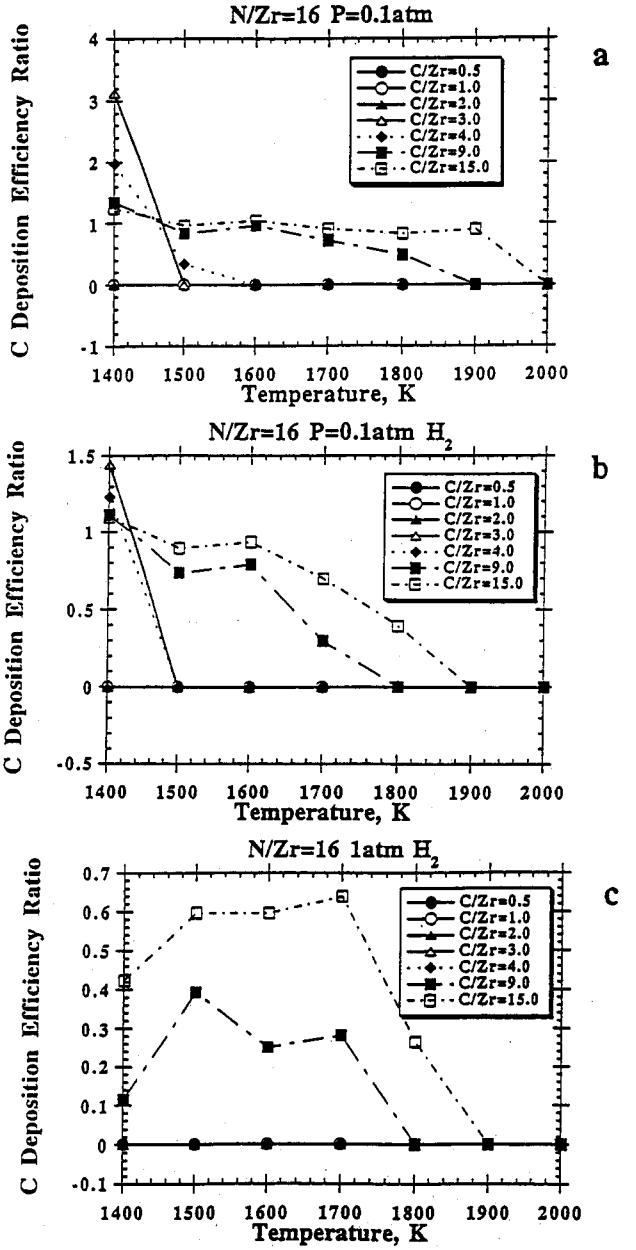

Figure 12. Effects of (a) low pressure (0.1 atm), (b) a combination of low pressure (P_{tot} = 0.1 atm) and excess hydrogen (50 mol), and (c) addition of excess hydrogen (50 mol, P_{tot} = 1 atm) on the C deposition efficiency ratio. The NH_3/ZrO_2 ratio was kept at 16. Each curve represents the conversion efficiency ratio response for a specific CH_4/ZrO_2 ratio as indicated in the figure.

the trends in the Zr conversion efficiency ratio are identical to those of the N conversion efficiency ratio. The ratios decrease rapidly at temperatures above 1600 K to a value of 1 (±0.5) at 1800 K. There is no enhanced Zr or N conversion efficiency above a reaction temperature of 1800 K, i.e., the ratio of the Zr and N conversion efficiencies with and without the addition of hydrogen remained at 1.0 for all CH_4/ZrO_2 ratios. In the case where P_{tot} = 1.0 atm and in the presence of excess hydrogen, the conversion efficiency ratios increase to a maximum value of 1.0 at temperatures above 1600 K for C/Zr ≤ 4. On the other hand, the ratios decrease to zero for C/Zr > 4 at temperatures above 1700 K, due to the formation of ZrC. The above observations suggest that a decrease in P_{tot} is more effective in enhancing the conversion of ZrO_2 to ZrN than the introduction of hydrogen into the system.

Effect of Low Pressure and Excess Hydrogen on C Deposition Efficiencies. Figure 9b shows the C deposition efficiency plots for P_{tot} = 0.1 atm. Decreasing the pressure results in the onset of C deposition at lower C/Zr ratios and at lower temperatures compared to that predicted at P_{tot} = 1.0 atm. The shapes of the deposition efficiency plots are also changed from those at P_{tot} = 1.0 atm. Plots for the system at P_{tot} = 1.0 atm in the presence of excess hydrogen have shapes similar to those at P_{tot} without the presence of excess hydrogen (compare Figure 9c with 9a). However, C deposition still occurs at lower temperatures and lower C/Zr ratio. Figure 9d shows that thermodynamic calculations predict that addition of hydrogen at P_{tot} = 1.0 atm eliminates C deposition for C/Zr ≤ 4. C deposition still occurs at C/Zr ≥ 9. However, the onset of C deposition

occurs at higher temperatures in the presence of hydrogen (compare Figure 9d with 9a).

Figure 12 summarizes the effects of low system pressure and/or addition of excess hydrogen on the C deposition efficiency ratios. For $P_{tot} = 0.1$ atm, no C deposition occurs at C/Zr ≤ 2. In the case in which 3 ≤ C/Zr ≤ 4, the C deposition efficiency ratio is initially greater than one at low reaction temperature (≤1500 K). In other words, more C is deposited at $P_{tot} = 0.1$ atm than at $P_{tot} = 1.0$ atm. However, the ratio decreases rapidly to zero as the reaction temperature increases above 1500 K, such that no C is deposited at temperatures of 1600 K and above. At $P_{tot} = 0.1$ atm the deposition efficiency ratio is about 1.0 for C/Zr ≥ 9. However, addition of excess hydrogen to the system decreases the deposition efficiency ratio to lower than 1.0 at temperatures above 1600 K. The deposition efficiency ratio decreases to zero at 1800 and 1900 K for C/Zr = 9 and C/Zr = 15, respectively. Introduction of hydrogen results in deposition efficiency ratios of less than 1.0 at $P_{tot} = 1.0$ atm for all C/Zr ratios. Thus, the effects of addition of excess hydrogen to the Zr–C–N system is to decrease or eliminate altogether C deposition.

Synthesis of Zirconium Nitride. Figure 13a shows the powder X-ray diffraction spectrum of the product obtained on heating the sol–gel powder to 1373 K for 12 h. The diffraction pattern corresponds to that of a mixture of oxides. Nitridation of the powder at 1323 K for 3 h results in the formation of ZrN as shown in Figure 13b. However, nitridation of the powder at lower temperatures, e.g., 1173 K for 3 h did not yield ZrN. The X-ray diffraction lines of the product for these conditions is monoclinic zirconium oxide. X-ray diffraction and surface analyses suggest that pure ZrN is formed for material heated to 1373 K for 12 h (13A). Such XRD data have a detection limit of about 5% for crystalline materials. Exactly why ZrN forms at temperatures below those predicted by our thermodynamic data is not known; however, it is clear that kinetics control the reaction process.

Conclusions

Computerized thermodynamic analysis of the Zr–N–C–H system indicates that pure ZrN can be prepared by thermal nitridation of ZrO_2 using ammonia and methane. Thermodynamic predictions reveal that complete conversion of ZrO_2 to ZrN occurs at 1800 K. The reagent concentration ranges within which pure ZrN is formed increase with increasing reaction temperature. Low pressure together with an excess of hydrogen decreases

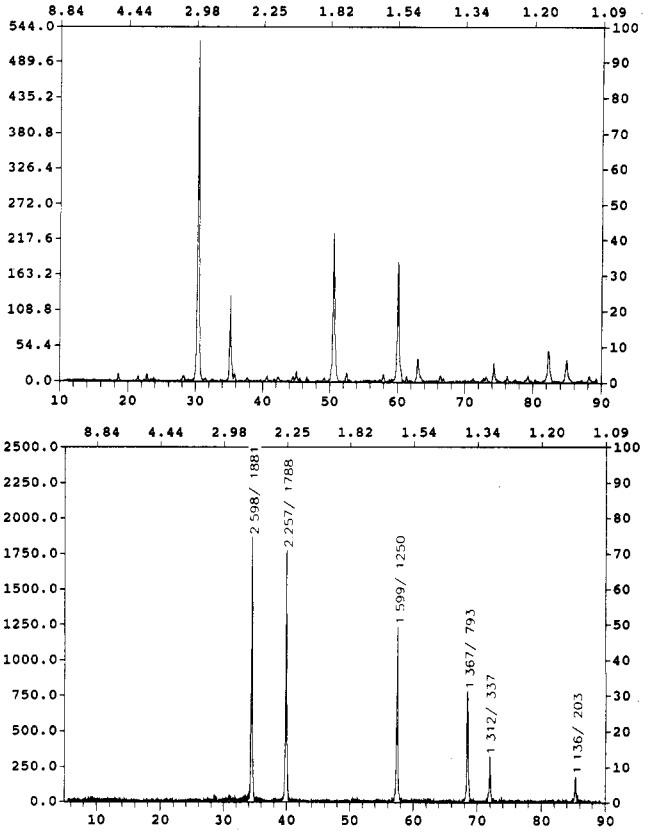

Figure 13. X-ray diffraction spectrum of (a) ZrO_2 powder obtained by calcining sol–gel precursor at 1100 °C in air for 12 h and (b) ZrN obtained by reacting the sol–gel precursor in ammonia and methane for 6 h at 1050 °C.

the reaction temperature at which pure ZrN is formed. Low pressure together with the introduction of excess hydrogen into the reaction system increases Zr and N conversion efficiency and retards C deposition. We have also shown experimentally, using reactant concentrations predicted by thermodynamic analysis, that zirconium nitride can indeed be formed by the thermal nitridation of zirconium oxide, using ammonia as the nitrogen source and methane as the reducing agent. However, the reaction temperature at which the conversion was achieved was 1323 K, much lower than that predicted from thermodynamic considerations alone.

Acknowledgment. This research has been supported by the State of Connecticut, Department of Higher Education, High Technology Grant Number 42.